Regular Rather than Chaotic Origin of the Resonant Transport in Superlattices

S. M. Soskin,[1,2,*] I. A. Khovanov,[3,4] and P. V. E. McClintock[2]
[1]Institute of Semiconductor Physics, National Academy of Sciences of Ukraine, 03028 Kiev, Ukraine
[2]Physics Department, Lancaster University, Lancaster LA1 4YB, United Kingdom
[3]School of Engineering, University of Warwick, Coventry CV4 7AL, United Kingdom
[4]Centre for Scientific Computing, University of Warwick, Coventry CV4 7AL, United Kingdom
(Received 12 September 2014; published 22 April 2015)

We address the enhancement of electron transport in semiconductor superlattices that occurs in combined electric and magnetic fields when cyclotron rotation becomes resonant with Bloch oscillations. We show that the phenomenon is regular in origin, contrary to the widespread belief that it arises through chaotic diffusion. The theory verified by simulations provides an accurate description of earlier numerical results and suggests new ways of controlling resonant transport.

DOI: 10.1103/PhysRevLett.114.166802 PACS numbers: 73.21.-b, 05.45.-a, 05.60.-k, 73.63.-b

Spatial periodicity plays a fundamental role in nature. In particular, it governs quantum electron transport in crystals [1]. In a perfect crystal lattice, an electron in a constant electric field would undergo Bloch oscillations, moving forwards and backwards periodically so that its average drift would be zero [1]. But real lattices are imperfect, and electrons may be scattered before reversing their motion, allowing them to acquire a steady drift. Typically, the Bloch oscillation period t_B greatly exceeds the average scattering time t_s, because t_B is proportional to the reciprocal of the lattice period d_l, which is very small. So, Bloch oscillations are not observed in real crystals. Nanoscale superlattices [2] (SLs) impose on the crystal an additional periodicity with a period d greatly exceeding d_l but still small enough for the quantum nature of the electron to be important: t_B may become comparable to or smaller than t_s so that Bloch oscillations can manifest themselves, significantly suppressing the current, generating gigahertz or terahertz electric signals, and causing other important effects [3,4].

The first description of electron drift in SLs [2] showed that the drift velocity v_d vs the electric field F along a one-dimensional SL possesses a peak at $F = F_{\mathrm{ET}}$ such that t_B (being $\propto F^{-1}$) is equal to t_s. It has important consequences, in particular, a peak in the differential conductivity vs voltage.

Another remarkable effect was predicted more recently [5,6]. It was noticed that, if a magnetic field is added, the dynamics reduces to that of an auxiliary classical harmonic oscillator at the cyclotron frequency subject to a traveling wave at the Bloch frequency. Numerical calculations within this model and the relaxation-time approximation for scattering [2] revealed additional peaks in $v_d(F)$ at the values of F corresponding to integer ratios between the Bloch and cyclotron frequencies. As is known from the theory of dynamical systems, the phase plane of a harmonic oscillator subject to a traveling wave is threaded by a so-called stochastic web if the ratio between the wave and oscillator frequencies is an integer [7,8]. This web plays an important role in many physical systems [9,10]. It was conjectured [5,6] that the dynamical origin of the peaks lies in chaotic diffusion along the web. This conjecture stimulated wide interest and numerous theoretical and experimental investigations of the effect and its applications (e.g., Refs. [11–21]). These and many other works (e.g., Refs. [22–27]) assumed the original conjecture to be correct, implying that resonant electron transport in SLs can be controlled by chaotic diffusion [18].

In the present Letter, we show that this commonly held belief is incorrect: the peaks originate in a regular dynamics, while chaos, when present, destroys them.

Consider a one-dimensional SL. Because of the periodicity, it possesses minibands [2]. Let the SL parameters be such that only the lowest miniband is relevant [5,6,11,13–21]. The electron energy can [5,6] be approximated as $E(\vec{p}) = \Delta[1-\cos(p_x d/\hbar)]/2 + (p_y^2 + p_z^2)/(2m^*)$, where $\vec{p} \equiv (p_x, p_y, p_z)$ is its quasimomentum, the x axis is directed along the SL, Δ is the miniband width, d is the SL period, and m^* is the electron effective mass for motion in the transverse plane. Let us apply an electric field antiparallel to the SL axis and a magnetic field tilted at an angle $\theta < 90°$: $\vec{F} = (-F, 0, 0)$ and $\vec{B} = (B\cos(\theta), 0, B\sin(\theta))$, respectively. The semiclassical equations of motion are [1–5,14,17–19,28]

$$\frac{d\vec{p}}{dt} = -e\{\vec{F} + [\vec{v} \times \vec{B}]\},$$
$$\vec{v} \equiv \left(\frac{dx}{dt}, \frac{dy}{dt}, \frac{dz}{dt}\right) = \left(\frac{\partial E}{\partial p_x}, \frac{\partial E}{\partial p_y}, \frac{\partial E}{\partial p_z}\right), \quad (1)$$

where e is the absolute value of the electronic charge.

The electron velocity in the x direction is

$$v_x(t) \equiv \frac{dx}{dt} = \frac{\partial E}{\partial p_x} = \frac{\Delta d}{2\hbar}\sin\left(\frac{p_x(t)d}{\hbar}\right). \tag{2}$$

Within the relaxation-time approximation [2], with a correction allowing for the difference between the elastic and inelastic scattering, the drift velocity is [3,6,37]

$$v_d = \mu\nu\int_0^\infty dt e^{-\nu t} v_x(t), \qquad \mu \equiv \sqrt{\frac{t_e}{t_e + t_i}}, \qquad \nu \equiv \frac{1}{\mu t_i}, \tag{3}$$

where t_e and t_i are the elastic and inelastic scattering times, respectively.

If $B = 0$, then $p_x(t) = eFt$. So, $v_x(t) \propto \sin(\omega_B t)$ where $\omega_B \equiv edF/\hbar$ is the Bloch frequency, and Eq. (3) gives the modified Esaki-Tsu (ET) result [2]:

$$v_d(F) \equiv v_{\mathrm{ET}}^{(\mathrm{mod})}(\omega_B) = v_0^{(\mathrm{mod})}\tilde{v}_{\mathrm{ET}}\left(\frac{\omega_B}{\nu}\right),$$
$$\omega_B \equiv \frac{ed}{\hbar}F, \qquad v_0^{(\mathrm{mod})} \equiv \mu\frac{\Delta d}{2\hbar}, \qquad \tilde{v}_{\mathrm{ET}}(x) \equiv \frac{x}{1+x^2}. \tag{4}$$

The function $\tilde{v}_{\mathrm{ET}}(\omega_B/\nu)$ (4) has a maximum at $\omega_B = \nu$.

If $B \neq 0$, the dynamics is much more complicated because the components of $\vec{p}$ are interwoven. Remarkably, however, the dynamics of p_z reduces to a relatively simple form, and p_x and p_y can be expressed in terms of p_z [5]. In terms of scaled quantities [19],

$$\frac{d^2\tilde{p}}{d\tilde{t}^2} + \tilde{p} = \epsilon\sin(\omega\tilde{t} - \tilde{p} + \phi_0),$$
$$\tilde{p} \equiv \tilde{p}_z(\tilde{t}) = p_z(t)\frac{d\tan(\theta)}{\hbar},$$
$$\tilde{t} \equiv \omega_c t, \qquad \omega_c \equiv \frac{eB\cos(\theta)}{m^*}, \qquad \omega \equiv \frac{\omega_B}{\omega_c},$$
$$\epsilon = \frac{\Delta m^*}{2}\left(\frac{d\tan(\theta)}{\hbar}\right)^2, \qquad \phi_0 = p_{z0} + p_{x0},$$
$$p_{z0} \equiv \tilde{p}_z(0), \qquad p_{x0} \equiv \tilde{p}_x(0), \qquad \tilde{p}_x(\tilde{t}) = p_x(t)\frac{d}{\hbar}. \tag{5}$$

Two other scaled components of the momentum are related to $\tilde{p}_z(\tilde{t}) \equiv \tilde{p}(\tilde{t})$ as follows: $\tilde{p}_x(\tilde{t}) = p_{x0} + \omega\tilde{t} - (\tilde{p}_z(\tilde{t}) - p_{z0})$ and $\tilde{p}_y(\tilde{t}) \equiv p_y(t)d/\hbar = d\tilde{p}_z(\tilde{t})/d\tilde{t}$.

The physical origin of the dynamics (5), its relevance to $v_x(t)$, and the physical meanings of ω_c and ϵ are as follows. The transverse component of the magnetic field and electron motion along the SL generate a Lorentz force oscillating at frequency ω_B. It excites a cyclotron rotation in the transverse plane which modulates p_x and, via p_x, the angle of the Bloch oscillation. The frequency of the cyclotron rotation, which we will call the cyclotron frequency, is ω_c. The amplitude of the Lorentz force in dimensionless units is ϵ. For details, see Ref. [28].

We consider the case of zero temperature, which is the most important one [5,6,13–21]. Only zero initial momenta are then relevant [5,17,19,28]. So, the scaled drift velocity reads as

$$\tilde{v}_d \equiv \frac{v_d}{v_0^{(\mathrm{mod})}} = \tilde{\nu}\int_0^\infty d\tilde{t} e^{-\tilde{\nu}\tilde{t}}\sin(\omega\tilde{t} - \tilde{p}), \qquad \tilde{\nu} \equiv \frac{\nu}{\omega_c}, \tag{6}$$

where $\tilde{p} \equiv \tilde{p}(\tilde{t})$ is a solution of Eq. (5) with

$$\tilde{p}(0) = 0, \qquad \frac{d\tilde{p}(\tilde{t}=0)}{d\tilde{t}} = 0, \qquad \phi_0 = 0, \tag{7}$$

and $\tilde{\nu}$ is the scattering rate in terms of the dimensionless "time" $\tilde{t}$ (5).

We will show that the resonance peak in $\tilde{v}_d(\omega)$ at $\omega \approx 1$ may be of magnitude ~ 1 for arbitrarily small ϵ. In contrast, the resonance contributions near multiple and rational frequencies necessarily vanish in the asymptotic limit $\epsilon \to 0$. These small contributions are ignored in our theory.

Necessary (but not sufficient) conditions for the distinct resonance peak are

$$\tilde{\nu} \ll 1, \qquad \epsilon/4 \ll 1. \tag{8}$$

If any of these conditions fail, the resonant component of $v_x(t)$ cannot accumulate for long. Besides, if the second condition fails, the peaks at multiple or rational frequencies are significant and/or the dynamics at the relevant time scales is chaotic. We assume further that the conditions (8) hold true unless otherwise specified.

As is clear from Eqs. (5)–(7), the function $\tilde{v}_d(\omega)$ depends on two parameters: $\tilde{\nu}$ and ϵ. But we show below that the magnitude and scaled shape of the resonance component depend only on a single parameter

$$\alpha \equiv \frac{\epsilon}{4\tilde{\nu}}. \tag{9}$$

It is proportional to the ratio of the two time scales—the scattering time and the time of the strong modulation of the Bloch oscillation angle—which in terms of dimensionless time (5) are $\tilde{t}_s = \tilde{\nu}^{-1}$ and $\tilde{t}_{\mathrm{SM}} = \epsilon^{-1}$, respectively. To illustrate the latter time scale, consider the exact resonance $\omega_B = \omega_c$. The modulation amplitude A_{am} then grows linearly with time, as $A_{\mathrm{am}} = \epsilon\tilde{t}/2$, until $A_{\mathrm{am}} \sim 1$. The latter range is reached just by $\tilde{t} \sim \tilde{t}_{\mathrm{SM}}$, and so strong modulation essentially changes the dynamics (5). However, if $\alpha \ll 1$, then the scattering occurs before the modulation becomes strong, so that the latter is irrelevant. Otherwise, the strong modulation comes into play, and the drift enhancement occurs differently.

We consider first the limit $\alpha \ll 1$. In this case, the magnitude of $\tilde{p}$ at the scattering time scale $\tilde{t}_s \equiv \tilde{\nu}^{-1}$ is $\sim\alpha \ll 1$, so that we can neglect $\tilde{p}$ in $\sin(\omega\tilde{t} - \tilde{p})$ on the rhs of the equation of motion (5), which then reduces to the

equation of the constrained vibration. Solving it with zero initial conditions (7) and substituting the result into the integrand of the integral (6), approximating $\sin(\omega\tilde{t}-\tilde{p})$ by $\sin(\omega\tilde{t})-\cos(\omega\tilde{t})\tilde{p}$, integrating, and neglecting asymptotically small terms, we obtain

$$\tilde{v}_d = \tilde{v}_{\mathrm{ET}}(\omega/\tilde{\nu}) + \tilde{v}_{d,a}^{(\mathrm{res})},$$
$$\tilde{v}_{d,a}^{(\mathrm{res})} = \alpha\frac{2\omega/(1+\omega)}{1+((\omega-1)/\tilde{\nu})^2}, \qquad \alpha \ll 1. \tag{10}$$

This is a superposition of the ET peak (4) and the resonance peak $\tilde{v}_{d,a}^{(\mathrm{res})}(\omega)$. The latter has an asymptotically Lorentzian shape with a half-width $\tilde{\nu}$ and maximum α acquired at $\omega = 1$. The physical origin of the peak is as follows. If $\omega_B = \omega_c$, the modulation amplitude of the Bloch oscillation angle grows with time, while the modulation-induced deviation of $v_x(t)$ possesses a component that retains its sign and also grows with time, thus, being accumulated. If $\omega_B - \omega_c \neq 0$, the modulation amplitude grows more slowly, and, moreover, if $|\omega_B - \omega_c| \gg \nu$, the sign of the deviation changes many times during t_s so that the drift averages to zero.

We now compare Eq. (10) with numerical simulations for the SL used in most experiments [6,11,13] and a typical magnetic field. So, let $d = 8.3$ nm, $\Delta = 19.1$ meV, $\nu = 4\times10^{12}$ s^{-1}, $m^* = 0.067m_e$ (where m_e is the free electron mass), and $B = 15$ T [13,19,20]. Then,

$$\tilde{\nu}\approx\frac{0.102}{\cos(\theta)}, \quad \epsilon\approx\frac{0.578}{\cot^2(\theta)}, \quad \alpha\approx1.42\frac{\sin^2(\theta)}{\cos(\theta)}. \tag{11}$$

Figure 1 presents the results for $\theta = 12°$ and 20°, where $\alpha = 0.063$ and 0.177, respectively. For $\theta = 12°$, the theory and simulations are virtually indistinguishable. For $\theta = 20°$, the theory only slightly exceeds the simulations.

As θ increases further, the excess of the theoretical resonant peak (10) over that in the simulations grows: $\tilde{v}_d(\omega = 1)$ in the simulations for $\theta = 40°$ [19,20] is about half that given by Eq. (10). The invalidity of Eq. (10) here is unsurprising because $\alpha \approx 0.77$ is not small.

To encompass arbitrary α, we develop an approach suggested earlier [7,8] in a different context. If $\omega \simeq 1$

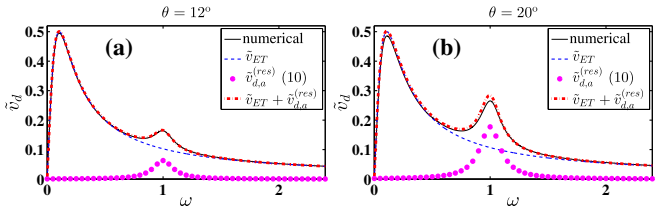

FIG. 1 (color online). Scaled drift velocity vs the ratio between the Bloch and cyclotron frequencies: comparison of numerical calculations (5)–(7) (black thin solid line) and the asymptotic theory (10) (red thick dash-dotted line) for (a) $\theta = 12°$, (b) $\theta = 20°$.

in Eq. (5), then, neglecting small fast oscillations, the dynamics reduces to that of the "resonant" Hamiltonian [7–10]:

$$H_r(I,\tilde{\varphi}) = -(\omega-1)I + \epsilon J_1(\rho)\cos(\tilde{\varphi}),$$
$$I = \frac{\tilde{p}^2+\dot{\tilde{p}}^2}{2}, \qquad \rho = \sqrt{2I},$$
$$\tilde{\varphi} = \varphi - \omega\tilde{t} + \pi, \qquad \varphi = \arctan\left(\frac{\tilde{p}}{\dot{\tilde{p}}}\right),$$
$$\tilde{p} = \rho\sin(\varphi), \qquad \dot{\tilde{p}} = \rho\cos(\varphi), \tag{12}$$

where $J_1(x)$ is a Bessel function of the first order [29].

If $|\omega-1|$ is sufficiently small, the Hamiltonian (12) possesses saddles generating separatrices [Figs. 2(a) and 2(b)]. When $\omega = 1$, the separatrices merge into a single infinite grid [Fig. 2(a)]. For the original system (5), the neglected fast-oscillating terms dress this grid with a chaotic layer, thus, forming a stochastic web (SW). Formally, chaotic diffusion along the vertical filaments of the SW might transport the system to arbitrarily high values of I, so that $|\vec{p}|$ might become arbitrarily large. In all former works, e.g., Refs. [5,6,11–27], it was this chaotic diffusion that was believed to be the origin of the resonant drift. This cannot be the case, however, because (i) at $\epsilon/4 \ll 1$, the time scale at which chaos manifests [7–10] is much larger than that for the formation of the resonant peak (being $\sim\omega_c^{-1}\min\{\tilde{t}_s,\tilde{t}_{\mathrm{SM}}\}$), and (ii) at $\epsilon/4 \gtrsim 1$, when chaos is pronounced, $\vec{p}$ varies chaotically at relevant time scales indeed, but this leads to a chaotic variation of the value and sign of v_x (2) in the integrand of the integral in Eq. (3), which decreases the integral rather than increasing it; therefore, chaos suppresses the drift.

We uncover the true origin of the resonant peak in the general case by an analysis of the regular dynamics along the trajectory of the resonant Hamiltonian (12) starting from $(I = +0, \tilde{\varphi} = \pi/2)$ [28]. In the equations of motion for the system (12), we transform from I to ρ and scale the time and frequency shift by the slow "time" $\tilde{t}_{\mathrm{SM}}$ and its reciprocal, respectively,

$$\frac{d\rho}{d\tau} = \frac{J_1(\rho)}{\rho}\sin(\tilde{\varphi}), \qquad \frac{d\tilde{\varphi}}{d\tau} = -\delta + \frac{\frac{dJ_1(\rho)}{d\rho}}{\rho}\cos(\tilde{\varphi}),$$
$$\tau \equiv \frac{\tilde{t}}{\tilde{t}_{\mathrm{SM}}} \equiv \epsilon\tilde{t}, \qquad \delta \equiv \frac{\omega-1}{\tilde{t}_{\mathrm{SM}}^{-1}} \equiv \frac{\omega-1}{\epsilon}. \tag{13}$$

For $|\omega-1| \ll 1$, the slow dymamics of $\tilde{p}$ is fully described by solution of Eq. (13) with appropriate initial conditions [28]

$$\rho(\tau=0) = +0, \qquad \tilde{\varphi}(\tau=0) = \pi/2. \tag{14}$$

The drift velocity is [28]

$$\tilde{v}_d = \tilde{v}_{\mathrm{ET}}(\omega/\tilde{\nu}) + \tilde{v}_d^{(\mathrm{res})}(\delta,\alpha),$$
$$\tilde{v}_d^{(\mathrm{res})} = \frac{\int_0^{\tau_p} d\tau \exp\left(-\frac{\tau}{4\alpha}\right)J_1[\rho(\tau)]\sin[\tilde{\varphi}(\tau)]}{4\alpha[1-\exp\left(-\frac{\tau_p}{4\alpha}\right)]}, \tag{15}$$

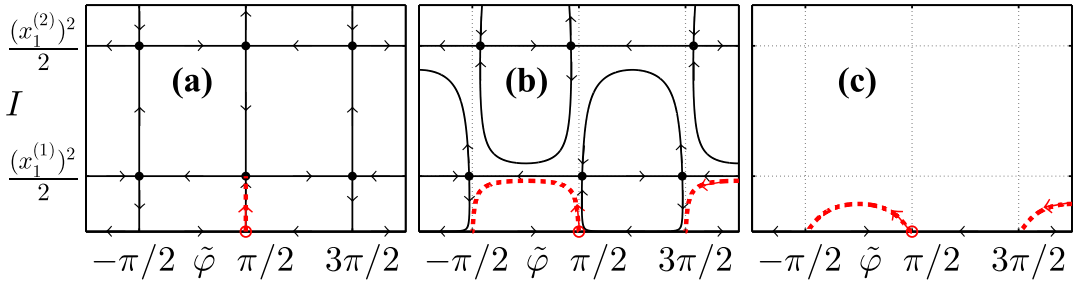

FIG. 2 (color online). Phase plane of the resonant Hamiltonian (12) for three characteristic values of $\delta \equiv (\omega - 1)/\epsilon$: (a) $\delta = 0$, (b) $0 < \delta < \delta_{\rm cr}^{(2)}$, (c) $\delta > \delta_{\rm cr}^{(1)}$, where $\delta_{\rm cr}^{(n)} = \{(1/x)|[dJ_1(x)/dx]|\}|_{x=x_1^{(n)}}$. The $x_1^{(n)}$ are nth zeros of the Bessel function $J_1(x)$. Red circles mark the points $(+0, \pi/2)$; the red dashed lines show outgoing trajectories [in (b),(c), the same applies to equivalent trajectories from $(+0, 5\pi/2)$]. Dots mark saddles; separatrices are shown by solid lines. Arrows indicate directions of motion.

where τ_p is the period of the trajectory (13) and (14). Figure 3 demonstrates the effectiveness of Eq. (15). Figure 3(a) relates to the aforementioned case (11) with $\theta = 40°$: the agreement between the theory and simulations in the range of the resonant peak is excellent. Figure 3(b) shows the evolution of $\tilde{v}_d(\omega)$ in the vicinity of $\omega = 1$ as α grows while $\tilde{\nu} = 0.02$. In addition to perfect agreement for $\epsilon \equiv 4\alpha\tilde{\nu} \lesssim 0.4$ and reasonable agreement for higher ϵ up to 0.8, it illustrates the key features discussed below.

A striking feature of Fig. 3(b) is the nonmonotonic dependence of the peak maximum on α. It is a consequence of an interplay between the time scales $\tilde{t}_s \equiv \tilde{\nu}^{-1}$ and $\tilde{t}_{\rm SM} \equiv \epsilon^{-1}$. To further clarify the role of the latter, consider the exact resonance: $\delta = 0$. The initial $\tilde{\varphi} = \pi/2$ is then preserved along the trajectory (13) and (14), so that ρ obeys the closed dynamical equation $d\rho/d\tau = J_1(\rho)/\rho$. At $\tau \equiv \tilde{t}/\tilde{t}_{\rm SM} \ll 1$, the rhs is equal to 1/2 [29], so that ρ reaches values ~ 1 for $\tau \sim 1$. The growth of ρ then slows down, and, for $\tau \sim 1$, ρ reaches the vicinity of $x_1^{(1)} \approx 4$ corresponding to the first saddle of the SW [Fig. 2(a)], where the growth saturates. Moreover, the stay in the vicinity of the saddle results in that resonant drift ceases. If $\tilde{t}_s \ll \tilde{t}_{\rm SM}$, the saturation of the ρ growth is irrelevant. So, increase of ϵ results in faster acceleration of the transverse momenta during the whole period before scattering, and, by the time of the scattering, their magnitude has reached higher values; the same applies to the modulation amplitude and, thus, $\tilde{v}_d^{(\rm res)}$ too. In the opposite limit $\tilde{t}_{\rm SM} \ll \tilde{t}_s$, the drift stops at $\tilde{t} \sim \tilde{t}_{\rm SM}$—long before the scattering. In this regime, the probability $P_{\rm RD}$ for electron to undergo the resonant drift is $\sim \tilde{t}_{\rm SM}/\tilde{t}_s$. Since $\tilde{v}_d^{(\rm res)}$ is proportional to $P_{\rm RD}$, it decreases together with $\tilde{t}_{\rm SM} \equiv \epsilon^{-1}$. The optimal regime is $\tilde{t}_s \sim \tilde{t}_{\rm SM}$, i.e., $\alpha \sim 1$.

Figure 4(a) shows the universal function $A(\alpha)$ representing the resonant peak maximum $\tilde{v}_d^{(\rm res)}(\delta = 0, \alpha)$ [the analytic formula is given in Eq. (S.6) of [28]]. It attains the maximum $A_{\rm max} \approx 0.38$ at $\alpha = \alpha_{\rm max} \approx 1.16$ while its small-α and large-α asymptotes are α and $(x_1^{(1)})^2/(8\alpha) \approx 1.84/\alpha$, respectively. Figure 4(b) compares $\tilde{v}_d(\omega = 1)$ and $\tilde{v}_{\rm ET}(1/\tilde{\nu}) + A[\epsilon/(4\tilde{\nu})]$ as functions of ϵ for a given $\tilde{\nu} = 0.02$. The agreement is excellent up to $\epsilon \approx 0.3$ and good up to $\epsilon \approx 0.7$.

Figure 3(b) demonstrates also that, as α increases, the width of the peak grows monotonically while its shape evolves from being domelike to being spikelike. Analytic results are presented in Ref. [28].

Finally, Fig. 3(b) demonstrates that chaos comes into play only at $\epsilon \sim 1$, leading to fluctuations in $\tilde{v}_d(\omega)$ (see the curve for $\alpha = 10$). As ϵ increases further, fluctuations intensify while the peak disappears [see the curve for $\alpha = 15$ and the range $\epsilon \gtrsim 1.2$ in Fig. 4(b)]. See Ref. [28] for

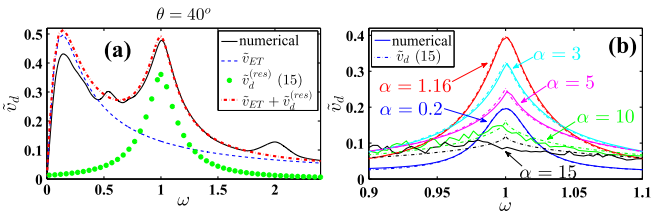

FIG. 3 (color online). Scaled drift velocity vs the ratio between the Bloch and cyclotron frequencies: the general theory (15) and the numerical simulations for (a) the case Eq. (11) with $\theta = 40°$, (b) $\tilde{\nu} = 0.02$ as $\alpha \equiv \epsilon/(4\tilde{\nu})$ increases.

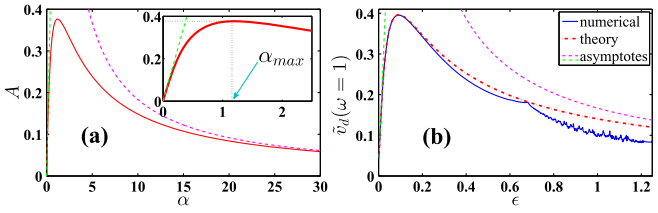

FIG. 4 (color online). (a) Universal asymptotic dependence (S.6) of the amplitude of the resonant peak on $\alpha \equiv \epsilon/(4\tilde{\nu})$ (solid line) and its asymptotes for small and large α (dashed lines). The inset shows the enlarged scale for $\alpha < 2.5$. (b) Comparison between (i) numerically calculated $\tilde{v}_d(\omega = 1)$ for $\tilde{\nu} = 0.02$ as a function of ϵ (blue thin solid lines) and (ii) the theory—the general theory (red dash-dotted line) i.e. Eq. (15) for $\omega = 1$ while $v_d^{(res)}(\omega = 1)$ reduces to the expression given in Eq. (S.6) of [28], and the small-α or large-α asymptotes (dashed lines) i.e. (15) for $\omega = 1$ while $v_d^{(res)}(\omega = 1)$ is approximated as α or $(x_1^{(1)})^2/(8\alpha)$ respectively.

details. Thus, chaos may be relevant only at $\epsilon \gtrsim 1$, playing a destructive role for the resonant drift, contrary to the established belief [5,6,11–27] about its constructive role. The latter belief suggested that the best performance of the resonant drift occurs when chaos is strong. However, neither simulations nor experiments [6,17,18,21] confirm this: as $\theta \to 90°$, when chaos intensifies to its maximum extent, the drift vanishes. Our work shows that the ways needed to control the resonant drift are different. If the model (1) is valid and $\tilde{\nu} \ll 1$ and $\epsilon/4 \ll 1$, it is controlled by a single parameter α. The best performance corresponds to $\alpha = \alpha_{\max} \approx 1.16$. The drift is negligible if any of the following conditions hold: $\alpha \lesssim 0.1$, $\alpha \gtrsim 20$, $\tilde{\nu} \gtrsim 1$. As ϵ grows above 1, the resonant drift at $\omega \approx 1$ gradually decays (at multiples, it first rises and then decays too). See Ref. [28] for illustrations.

In conclusion, we have shown that the enhancement of the electron drift occurring if the Bloch and cyclotron frequencies are close, originates in a regular dynamics, contrary to the widespread belief that its origin is in chaotic diffusion. The enhancement is explained as follows. The electron motion along the SL and the tilted magnetic field produce a Lorentz force oscillating at the Bloch frequency. It excites cyclotron rotation which modulates the angle of the Bloch oscillation of the instantaneous velocity. Beyond resonance, the velocity change caused by the modulation oscillates during the relevant time scale, and so the drift averages to zero. In contrast, the change in the resonant case keeps its sign, thus, being accumulated.

Discussions with Vladimir Kravtsov, Oleg Yevtushenko, Boris Glavin, and Oleg Raichev are much appreciated. S. M. S. acknowledges the CMSP section of the Abdus Salam International Centre for Theoretical Physics for the support of his visit there when a part of the Letter was prepared. The research was supported in part by the Engineering and Physical Sciences Research Council UK (Grant No. EP/G070660/1).

*stanislav.soskin@gmail.com

[1] N. W. Ashcroft and N. D. Mermin, *Solid State Physics* (Holt, Reinhart and Winston, New York, 1976).

[2] L. Esaki and R. Tsu, Superlattice and negative differential conductivity in Semiconductors, IBM J. Res. Dev. **14**, 61 (1970).

[3] A. Wacker, Semiconductor superlattices: a model system for nonlinear transport, Phys. Rep. **357**, 1 (2002).

[4] R. Tsu, *Superlattices to Nanoelectronics* (Elsevier, Amsterdam, 2002).

[5] T. M. Fromhold, A. A. Krokhin, C. R. Tench, S. Bujkiewicz, P. B. Wilkinson, F. W. Sheard, and L. Eaves, Effects of Stochastic Webs on Chaotic Electron Transport in Semiconductor Superlattices, Phys. Rev. Lett. **87**, 046803 (2001).

[6] T. M. Fromhold, A. Patane, S. Bujkiewicz, P. B. Wilkinson, D. Fowler, D. Sherwood, S. P. Stapleton, A. A. Krokhin, L. Eaves, M. Henini *et al.*, Chaotic electron diffusion through stochastic webs enhances current flow in superlattices, Nature (London) **428**, 726 (2004).

[7] A. A. Chernikov, M. Y. Natenzon, B. A. Petrovichev, R. Z. Sagdeev, and G. M. Zaslavsky, Some peculiarities of stochastic layer and stochastic web formation, Phys. Lett. A **122**, 39 (1987).

[8] A. A. Chernikov, M. Y. Natenzon, B. A. Petrovichev, R. Z. Sagdeev, and G. M. Zaslavsky, Strong changing of adiabatic invariants, KAM-tori and web-tori, Phys. Lett. A **129**, 377 (1988).

[9] G. M. Zaslavsky, R. Z. Sagdeev, D. A. Usikov, and A. A. Chernikov, *Weak Chaos and Quasi-Regular Patterns* (Cambridge University Press, Cambridge, England, 1991).

[10] G. M. Zaslavsky, *Physics of Chaos in Hamiltonian Systems* (Imperial College Press, London, 2007).

[11] A. Patane, D. Sherwood, L. Eaves, T. M. Fromhold, M. Henini, and P. C. Main, Tailoring the electronic properties of GaAs/AlAs superlattices by InAs layer insertions, Appl. Phys. Lett. **81**, 661 (2002).

[12] D. P. A. Hardwick, S. L. Naylor, S. Bujkiewicz, T. M. Fromhold, D. Fowler, A. Patanè, L. Eaves, A. A. Krokhin, P. B. Wilkinson, M. Henini, F. W. Sheard, Effect of inter-miniband tunneling on current resonances due to the formation of stochastic conduction networks in superlattices, Physica E **32**, 285 (2006).

[13] D. Fowler, D. P. A. Hardwick, A. Patane, M. T. Greenaway, A. G. Balanov, T. M. Fromhold, L. Eaves, M. Henini, N. Kozlova, J. Freudenberger *et al.*, Magnetic-field-induced miniband conduction in semiconductor superlattices, Phys. Rev. B **76**, 245303 (2007).

[14] A. G. Balanov, D. Fowler, A. Patane, L. Eaves, and T. M. Fromhold, Bifurcations and chaos in semiconductor superlattices with a tilted magnetic field, Phys. Rev. E **77**, 026209 (2008).

[15] N. V. Demarina, E. Mohler, A. Lisauskas, and H. G. Roskos, Magnetic-field-enhanced transient and stationary drift currents of oscillating Bloch electrons in superlattices and limits of average-particle description in relation to Monte Carlo simulations, Phys. Rev. B **80**, 245307 (2009).

[16] M. T. Greenaway, A. G. Balanov, E. Scholl, and T. M. Fromhold, Controlling and enhancing terahertz collective electron dynamics in superlattices by chaos-assisted miniband transport, Phys. Rev. B **80**, 205318 (2009).

[17] T. M. Fromhold, A. A. Krokhin, S. Bujkiewicz, P. B. Wilkinson, D. Fowler, A. Patane, L. Eaves, D. P. A. Hardwick, A. G. Balanov, M. T. Greenaway *et al.*, in *Hamiltonian Chaos Beyond the KAM Theory*, edited by A. C. J. Luo and V. Afraimovich (Higher Education Press and Springer, Beijing, 2010), pp. 225–254.

[18] S. M. Soskin, P. V. E. McClintock, T. M. Fromhold, I. A. Khovanov, and R. Mannella, Stochastic webs and quantum transport in superlattices: an introductory review, Contemp. Phys. **51**, 233 (2010).

[19] A. O. Sel'skii, A. A. Koronovskii, A. E. Hramov, O. I. Moskalenko, K. N. Alekseev, M. T. Greenaway, F. Wang, T. M. Fromhold, A. V. Shorokhov, N. N. Khvastunov *et al.*, Effect of temperature on resonant electron transport through stochastic conduction channels in superlattices, Phys. Rev. B **84**, 235311 (2011).

[20] A. G. Balanov, M. T. Greenaway, A. A. Koronovskii, O. I. Moskalenko, A. O. Sel'skii, T. M. Fromhold, and

A. E. Khramov, The effect of temperature on the nonlinear dynamics of charge in a semiconductor superlattice in the presence of a magnetic field, JETP Lett. **114**, 836 (2012).

[21] N. Alexeeva, M. T. Greenaway, A. G. Balanov, O. Makarovsky, A. Patane, M. B. Gaifullin, F. Kusmartsev, and T. M. Fromhold, High-frequency collective electron dynamics via single-particle complexity, Phys. Rev. Lett. **109**, 024102 (2012).

[22] Y. A. Kosevich, A. B. Hummel, H. G. Roskos, and K. Kohler, Ultrafast Fiske Effect in Semiconductor Superlattices, Phys. Rev. Lett. **96**, 137403 (2006).

[23] R. G. Scott, S. Bujkiewicz, T. M. Fromhold, P. B. Wilkinson, and F. W. Sheard, Effects of chaotic energy-band transport on the quantized states of ultracold sodium atoms in an optical lattice with a tilted harmonic trap, Phys. Rev. A **66**, 023407 (2002).

[24] R. G. Scott, A. M. Martin, T. M. Fromhold, S. Bujkiewicz, F. W. Sheard, and M. Leadbeater, Creation of solitons and vortices by Bragg reflection of Bose-Einstein condensates in an optical lattice, Phys. Rev. Lett. **90**, 110404 (2003).

[25] O. Morsch and M. Oberthaler, Dynamics of Bose-Einstein condensates in optical lattices, Rev. Mod. Phys. **78**, 179 (2006).

[26] P. Wilkinson and M. Fromhold, Chaotic ray dynamics in slowly varying two-dimensional photonic crystals, Opt. Lett. **28**, 1034 (2003).

[27] A. J. Henning, T. M. Fromhold, and P. B. Wilkinson, Using dynamical barriers to control the transmission of light through slowly varying photonic crystals, Phys. Rev. E **83**, 046209 (2011).

[28] See Supplemental Material at http://link.aps.org/supplemental/10.1103/PhysRevLett.114.166802, which includes Refs. [29–36], for a discussion of the physical origin of the dynamics and initial conditions; a general analytic treatment of the resonant peak; additional details about the role of chaos; and illustrations of control over the drift.

[29] M. Abramovitz and I. A. Stegun, *Handbook of Mathematical Functions* (Dover, New York, 1972).

[30] A. A. Krokhin, T. M. Fromhold, A. E. Belyaev, H. M. Murphy, L. Eaves, D. Sherwood, P. C. Main, and M. Henini, Suppression of electron injection into a finite superlattice in an applied magnetic field, Phys. Rev. B **63**, 195323 (2001).

[31] L. D. Landau and E. M. Lifshitz, *Quantum Mechanics (Non-Relativistic Theory)*, Course of Theoretical Physics, 3rd ed. Vol. 3, with corrections, translated from Russian, edited by J. B. Sykes and J. S. Bell (Butterworth-Heinemann, Oxford, 1991).

[32] A. Wacker and A. P. Jauho, Quantum Transport: The Link Between Standard Approaches in Superlattices, Phys. Rev. Lett. **80**, 369 (1998).

[33] S. Glutsch, Nonresonant and resonant Zener tunneling, Phys. Rev. B **69**, 235317 (2004).

[34] G. Belle, J. C. Maan, and G. Weimann, Measurement of the miniband width in a superlattice with interband absorption in a magnetic field parallel to the layers, Solid State Commun. **56**, 65 (1985).

[35] Yu. A. Kosevich, Anomalous Hall velocity, transient weak supercurrent, and coherent Meissner effect in semiconductor superlattices, Phys. Rev. B **63**, 205313 (2001).

[36] *Semiconductors: Data Handbook*, edited by O. Madelung (Springer, Heidelberg, 2004).

[37] A. A. Ignatov, E. P. Dodin, and V. I. Shashkin, Transient response theory of semiconductor lattices: connection with Bloch oscillations, Mod. Phys. Lett. B **05**, 1087 (1991).